Published in final edited form as:
Neuron. 2011 June 23; 70(6): 1100–1114. doi:10.1016/j.neuron.2011.04.031.

Overlapping Role of Dynamin Isoforms in Synaptic Vesicle Endocytosis

Andrea Raimondi[1,§,*], **Shawn M. Ferguson**[1,*,‡], **Xuelin Lou**[1], **Moritz Armbruster**[2,3], **Summer Paradise**[1], **Silvia Giovedi**[1], **Mirko Messa**[1], **Nao Kono**[1], **Junko Takasaki**[1], **Valentina Cappello**[1,$], **Eileen O'Toole**[4], **Timothy A. Ryan**[2], and **Pietro De Camilli**[1,‡]

[1]Department of Cell Biology, HHMI, Program in Cellular Neuroscience, Neurodegeneration and Repair and Kavli Institute for Neuroscience, Yale University School of Medicine, New Haven, CT, USA

[2]Department of Biochemistry, Weill Cornell Medical College, New York

[3]David Rockefeller Graduate Program, The Rockefeller University, New York, NY

[4]Laboratory for 3D Electron Microscopy of Cells, MCDP Department, University of Colorado, Boulder, CO 80309, USA

Abstract

The existence of neuron specific endocytic protein isoforms raises questions about their importance for specialized neuronal functions. Dynamin, a GTPase implicated in the fission reaction of endocytosis, is encoded by three genes, two of which, dynamin 1 and 3, are highly expressed in neurons. We show that dynamin 3, thought to play a predominantly postsynaptic role, has a major presynaptic function. While lack of dynamin 3 does not produce an overt phenotype in mice, it worsens the dynamin 1 KO phenotype, leading to perinatal lethality and a more severe defect in activity-dependent synaptic vesicle endocytosis. Thus, dynamin 1 and 3, which together account for the overwhelming majority of brain dynamin, cooperate in supporting optimal rates of synaptic vesicle endocytosis. Persistence of synaptic transmission in their absence indicates that if dynamin plays essential functions in neurons, such functions can be achieved by the very low levels of dynamin 2.

Introduction

Clathrin mediated endocytosis is an evolutionarily conserved process that cells use to internalize specific components of the plasma membrane (Conner and Schmid, 2003; Doherty and McMahon, 2009). In higher eukaryotes, clathrin mediated endocytosis plays particularly important and specialized functions at neuronal synapses (Dittman and Ryan, 2009; Murthy and De Camilli, 2003). On the presynaptic side, it is implicated in the recycling of synaptic vesicle membranes (Dittman and Ryan, 2009; Granseth et al., 2006; Jung and Haucke, 2007; Murthy and De Camilli, 2003). On the postsynaptic side, it

‡To whom correspondence should be addressed. shawn.ferguson@yale.edu or pietro.decamilli@yale.edu .
§Current address: Neuroscience and Brain Technology Department, IIT, Genova.
$Current address: Department of Medical Pharmacology, University of Milano, Milano, Italy
*Both authors contributed equally to this work

mediates the internalization of neurotransmitter receptors and thus contributes to synaptic plasticity by controlling postsynaptic excitability (Carroll et al., 1999; Chowdhury et al., 2006; Petrini et al., 2009; Shepherd and Huganir, 2007).

The use of a house-keeping process for specialized aspects of neuronal function implies the occurrence of unique adaptations. Several clathrin coat components and their accessory factors are encoded by multiple genes that undergo alternative splicing, some of which are exclusively or preferentially expressed in brain (Blondeau et al., 2004; Cao et al., 1998; Hirst and Robinson, 1998; Stamm et al., 1992; Tebar et al., 1999). An important question is whether these variants are localized in distinct compartments of the neuronal cytoplasm and have fundamentally distinct roles, or whether they have overlapping functions.

An endocytic protein that plays a key function in the fission reaction of clathrin-mediated endocytosis and which is expressed as different isoforms in mammals is the GTPase dynamin (Cao et al., 1998; Praefcke and McMahon, 2004; Pucadyil and Schmid, 2009). In mammals, dynamin is encoded by three different genes (DNM1, DNM2 and DNM3), whose products undergo further alternative splicing to generate a multiplicity of variants (Cao et al., 1998). Dynamin 1 is highly and selectively expressed in the nervous system and represents by far the major dynamin isoform expressed in this tissue, where the total dynamin levels far exceed those present in other tissues (Ferguson et al., 2007). Dynamin 2 is ubiquitously expressed in all tissues (Cao et al., 1998; Ferguson et al., 2007). Dynamin 3 is most strongly expressed in the brain, but at concentrations that are much lower than dynamin 1 (Cao et al., 1998; Ferguson et al., 2007; Gray et al., 2003). Because of these patterns of expression, it had been speculated that dynamin 2 performs house-keeping functions, and that dynamin 1 is the dynamin selectively implicated in synaptic vesicle recycling. In contrast, dynamin 3 was reported to be highly concentrated post-synaptically and was proposed to have a preferential function in the control of endocyosis within dendritic spines and excitatory neurotransmitter receptor trafficking (Gray et al., 2003; Lu et al., 2007).

However, several observations suggest that the neuronal functions of dynamin 1 and dynamin 3, and possibly also of dynamin 2 are overlapping. The generation and characterization of dynamin 1 KO mice revealed that synaptic vesicles still form under conditions of moderate neuronal activity in these mice (Ferguson et al., 2007; Hayashi et al., 2008; Lou et al., 2008), thus ruling out an essential function for dynamin 1 in this process. Studies of dynamin 1 KO neurons further showed that a major role for the very high concentrations of dynamin in neurons, is to allow scaling of the rate of endocytosis when the endocytic load is increased as a result of increased synaptic vesicle exocytosis (Ferguson et al., 2007; Lou et al., 2008). Additionally, in dynamin 1 knockout neurons, endogenous dynamin 3 was seen to accumulate within presynaptic terminals, possibly reflecting a build-up of endocytic intermediates due to lack of dynamin 1 and a role of dynamin 3 in their fission (Ferguson et al., 2007; Hayashi et al., 2008). These results challenged the proposed predominantly postsynaptic role for dynamin 3 at excitatory synapses.

In this study, we used a genetic model to investigate the possibility of overlapping actions of dynamin 1 and 3 in presynaptic function and by extension to also gain insight into the potential contributions of dynamin 2. We show that lack of dynamin 3 alone in mice does not produce an obvious pathological phenotype while the combined absence of dynamin 1 and 3 produces defects at the organism and cellular level that demonstrate an overlapping role of these two dynamin isoforms in synaptic vesicle endocytosis. Surprisingly, the extremely low levels of neuronal dynamin accounted for by dynamin 2 appear to be sufficient to support neuronal life and synaptic transmission. These results also raise the

possibility that dynamin-independent mechanisms may allow a basic form of synaptic vesicle recycling.

Results

Shared properties dynamin 1 and 3

We have previously shown that endogenous dynamin 3 accumulated within presynaptic terminals in dynamin 1 KO neurons, possibly reflecting a build-up of endocytic intermediates and a role of dynamin 3 in their fission (Ferguson et al., 2007; Hayashi et al., 2008). Consistent with an overlapping function of dynamin 1 and 3 in nerve terminals, antibodies that specifically recognize either dynamin 1 or dynamin 3 (Fig. S1A-C and Fig. 1E respectively), revealed a similar subcellular localization of these two proteins in brain with a diffuse localization throughout the cytoplasm and an accumulation at synapses (Fig. 1A).

If dynamin 1 and 3 perform overlapping functions, they would be expected to share at least a set of binding partners. The most prominent dynamin binding partners contain SH3 domains that bind short motifs within the C-terminal proline rich domain (PRD) of dynamin (Anggono and Robinson, 2007; Slepnev et al., 1998). The conservation of such interactions between dynamin 1, 2 and 3 has not previously been investigated in side-by-side comparisons. To address this issue, the core PRD regions of the three dynamins were used as baits in GST pulldowns from brain extracts (Fig. 1B). Western blotting of the affinity-purified material demonstrated that all proteins enriched on dynamin 1 PRD beads, such as BAR and F-BAR domain containing proteins (endophilin, amphiphysin, SNX9 and syndapin), intersectin and Grb2, were retained on the dynamin 3 PRD, while greater variability was observed for the material retained on the dynamin 2 PRD beads, suggesting greater similarities in the roles of dynamin 1 and 3 relative to those of dynamin 2.

Dynamin 3 KO mice do not exhibit obvious defects

To directly test the function of dynamin 3, we generated a mouse dynamin 3 conditional (floxed) KO allele (Fig. S1D). Mating of the heterozygous conditional KO mice to a Cre deleter strain (Lewandoski et al., 1997) yielded heterozygous KO mice that were bred to each other. Wild type, heterozygous and dynamin 3 KO pups were born in the expected 1:2:1 Mendelian ratio (26:48:20 from 12 litters genotyped at the time of weaning; $p=0.67$, χ^2 test) and the KO mice were grossly healthy, viable and fertile. Western blotting with antibodies directed against the C-terminal region of dynamin 3 (Ferguson et al., 2007) confirmed the absence of the protein in brain, testis and lung; i.e. the tissues where it is most prominently expressed (Fig. 1C). Due to the high levels of dynamin 1, dynamin 3 represents only a minor fraction of the total dynamin in the brain (Ferguson et al., 2007). However, Western blotting with a antibody that specifically and equally recognizes both dynamin 2 and 3 (Ferguson et al., 2009) showed that dynamin 3 makes a larger contribution to total dynamin levels in the brain than does dynamin 2, which in turn is expressed at lower concentration in brain than in other tissues (Fig. 1C). In spite of the expression of dynamin 3 in the testis and of its proposed function in sperm maturation (Vaid et al., 2007), matings between dynamin 3 KO mice yielded pups without any indication of fertility defects (see below).

As expected, the immunoreactivity recognized by our anti-dynamin 3 rabbit polyclonal and mouse monoclonal (clone 5H5) antibodies was no longer observed in KO samples (Fig. 1A, C and E). In contrast, the fluorescence produced by a more widely used dynamin 3 antibody that strongly labels dendritic spines (Gray et al., 2003; Lu et al., 2007) was unchanged in

dynamin 3 KO neurons (Fig. 1E). Thus, these experiments do not support the reported preferential postsynaptic localization of dynamin 3 in dendritic spines.

Consistent with their overall good health, no defects were observed in the brain of dynamin 3 KO mice at the histological level (data not shown). Likewise, no defects were observed in primary cultures of cortical neurons with respect to gross morphology or distribution of immunoreactivity for synaptic markers, including clathrin coat components (α-adaptin), synaptic vesicle proteins (synapsin; as well as synaptophysin and synaptobrevin, not shown) and an active zone protein (Bassoon) (Fig. 1D). Furthermore, electron microscopy analysis of dynamin 3 KO synapses in primary neuronal cultures did not reveal obvious pre- or post-synaptic structural alterations (Fig. 1F). For example, synaptic vesicles were abundant and showed a normal homogeneous diameter.

Synthetic neonatal lethal phenotype of dynamin 1/3 double KO (DKO) mice

To test for a synergistic function of dynamin 1 and 3, mice harboring KO alleles of dynamin 1 and 3 were bred to yield double KO (DKO) mice. Such mice were born, but were immediately distinguishable from their littermates because of their limited movement. They failed to nurse and died within several hours after birth (Fig. 2A). Thus, they had a more severe phenotype than dynamin 1 single KO mice that can survive for up to 2 weeks (Ferguson et al., 2007).

The survival of DKO mice for several hours after birth indicates that synaptic transmission must occur in at least a limited form in the absence of both dynamin 1 and 3. Accordingly, electron microscopy analysis of neonatal DKO brain stem synapses (Fig. 2C and D) and neuromuscular junctions (Fig. S2) revealed the presence of synaptic vesicles, although such vesicles were in general more heterogeneous in size and less numerous than in controls (see below). Clathrin coated endocytic intermediates were also evident (Fig. 2D). Furthermore, cortical neuron primary cultures derived from brains of DKO newborn mice developed and established synapses *in vitro* with no obvious differences from controls in morphology and synaptic density (see below), in spite of the extremely low level of total dynamin remaining (accounted for by dynamin 2) relative to control cultures (Fig. 2B). The actual contribution of neuronal dynamin 2 to the total dynamin pool detected in the cultures is expected to be even lower due to the presence of astrocytes, a cell type where dynamin 2 is more robustly expressed (Ferguson et al., 2007).

Levels of a variety of other synaptic proteins tested by Western blotting of such cultures, including: clathrin coat components, other endocytic proteins, synaptic vesicle proteins and cytoskeletal proteins were not changed in a significant way relative to controls (Fig. 2E). A significant decrease, however, was observed in the levels of Rab3, syndapin/pacsin 1, sorting nexin 9 (SNX9) as well as of parvalbumin and the vesicular GABA transporter (VGAT), two makers of GABA-ergic interneurons (Fig. 2E). Levels of gluatamic acid decarboxylase 65 (GAD65), another specific component of GABAergic neurons) were also decreased, although this decrease was just above the limit of significance (t test, $p = 0.056$). Loss of Rab3 may reflect excess degradation of this protein in the absence of synaptic vesicles, while loss of parvalbumin VGAT and GAD65 may indicate selective vulnerability of GABA-ergic interneurons due to their high level of tonic activity. Decreased levels of syndapin and SNX9 may arise from the property of these proteins to form complexes with dynamin, and thus their destabilization in the absence of dynamin 1 and 3, although other dynamin interacting proteins such as amphiphysin 1, amphiphysin 2 and endophilin 1 maintained their normal levels. Syndapin is a major dynamin binding partner in neurons, and the partner whose interaction with dynamin 1 is regulated by Cdk5-dependent phosphorylation and calcineurin-dependent dephosphorylation of dynamin 1 (Anggono et al., 2006). Phosphorylation on conserved sites within dynamin 3 suggests that similar

regulatory mechanisms may control dynamin 3 functions and interactions (Larsen et al., 2004).

Synaptic transmission at DKO synapses

The properties of synaptic transmission in DKO neurons were assessed in primary neuronal cultures obtained from newborn pups as this experimental system allows neurons and synapses to undergo a maturation that is not achievable in the intact mice due to their perinatal lethality. No obvious defects were observed in the overall development and morphology of the DKO cultures relative to control cultures, as assessed by bright field microscopy observations, immunofluorescence staining for markers of general neuron morphology (cytoskeletal proteins), axons (tau), dendrites (MAP2) as well as pre- (bassoon) and post-synaptic (PSD95) markers of synaptic junctions (Fig. S3).

Electrophysiological recordings from the cultures after 10-14 days *in vitro* (DIV) revealed that miniature excitatory postsynaptic current (mEPSCs) were present (Fig. 3A), although their amplitude was more variable (Fig. 3B and D, co-efficients of variance were 0.28 and 0.45 for control and DKO respectively), average charge transfer (Q) was slightly increased relative to controls (Fig. 3E) and their frequency slightly decreased (Fig. 3C). Local field stimulation also evoked synaptic currents (Fig. 3F). However, on average, these EPSCs were much smaller in amplitude in the DKO cultures (Fig. 3G). As overall synapse density as assessed by bassoon (Fig. S3E and F) and PSD-95 immunostaining (Fig. 5C) was maintained in the DKO neuron cultures, this decrease in EPSC amplitude could be explained by a decreased availability of synaptic vesicles in the absence of dynamin 1 and 3. Thus, the additional KO of dynamin 3 worsens the defect in the efficiency of synaptic transmission observed at dynamin 1 KO synapses, where the EPSC amplitude was shown to be better maintained (Ferguson et al., 2007; Lou et al., 2008). However, these results show that, surprisingly, synaptic transmission can occur in the absence of both dynamin 1 and 3, when dynamin levels are very low and accounted for by dynamin 2.

Severe defects in compensatory synaptic vesicle endocytosis

To directly investigate synaptic vesicle recycling dynamics, measurements of recycling parameters were performed using vGlut1-pHluorin in wild type, dynamin 1 KO, dynamin 3 KO and DKO neurons (Fig. 4). vGlut1-pHluorin is a pH sensitive probe that is very efficiently targeted to synaptic vesicles (Balaji and Ryan, 2007). Neurons transfected with vGlut1-pHluorin were selected for analysis based on their ability to respond to repeated rounds of stimulation. Microscopic inspection revealed that, in general, both dynamin 1 KO and DKO neurons had much higher baseline vGlut1-pHluorin fluorescence than either the wild type or the dynamin 3 KO neurons, which were indistinguishable from one another (Fig. 4A). NH_4Cl and acid-surface quenching (Fig. S4) demonstrated that this difference was due to a much higher fraction of vGlut1-pHluorin present on the plasma membrane consistent with a steady-state impairment of endocytic function. Following a stimulus-evoked increase in fluorescence due to synaptic vesicle exocytosis, the vGlut1-pHluorin signal gradually returned to baseline in all 4 genotypes (Fig. 4B). While the recovery was not affected by the KO of dynamin 3, the KO of dynamin 1 resulted in a small but statistically significant defect in the post-stimulus recovery. Importantly, the delay in recovery was much more severe in the DKO neurons (Fig. 4B). The $t_{1/2}$ recovery times following 100 AP at 10 Hz stimuli were 16.9+/−1.1 seconds for wildtype, 15.2+/−3.1 seconds for the dynamin 3 KO, 22.9+/−1.7 seconds for the dynamin 1 KO and 82.3+/−20.4 seconds for the DKOs, respectively. Importantly, given sufficient time, the signal did recover in DKO neurons and their synapses could sustain multiple rounds of exocytosis and endocytosis (Fig. 4C). Multiple stimulations of the same neuron also revealed that the time required for the vGlut1-pHluorin signal to return to baseline was quite variable from run to

run in DKOs (Fig 4D): the example of Fig. 4C shows 3 sequential rounds of stimulation and recovery whose $t_{1/2}$ varied from 62s to >140 s. This scale of variability was observed in all cells and was unrelated to previous history of stimulus recovery. Examination of all stimulus runs performed with a 100 AP stimulus at 10 Hz revealed that ~60% of the time the vGlut1-pHluorin signal required greater than 140 s to recover, but occasionally recovery could occur at WT speeds (Fig. 4D). These slow recoveries were not simply a reflection of a slow re-acidification step, as the fluorescence during the recovery period could be fully quenched by perfusion with a solution of pH 5.5 (Fig. S4). While the recovery in the dynamin 1 single KO was also slowed, the recovery was always complete within the 140 s post-stimulation time window.

Finally, a bafilomycin-based strategy that allows for separation of exocytic and endocytic contributions to the fluorescence traces (Sankaranarayanan and Ryan, 2001) demonstrated a complete lack of endocytosis during the 10 Hz stimulus train at DKO synapses (Fig. 4E and F), as was previously observed (Ferguson et al., 2007), and now reconfirmed (Fig. 4F), at dynamin 1 KO synapses. In contrast, the loss of dynamin 3 alone had no effect (Fig. 4F). Collectively these results demonstrate that the combined absence of dynamins 1 and 3 has dramatic synergistic effects on the kinetics of synaptic vesicle endocytosis but, perhaps more surprisingly, show that the DKO synapses still recycled their synaptic vesicles albeit at a much reduced rate.

A robust clustering of endocytic proteins within presynaptic terminals

DKO synapses in neuronal cultures were further carefully analyzed to assess the presence and abundance of endocytic intermediates. Studies of dynamin 1 KO nerve terminals in primary neuronal cultures had demonstrated an accumulation of presynaptic clathrin-coated pits that could be detected by immunofluorescence because it resulted in the enhanced clustering of immunoreactivity for clathrin coat components at synapses (Ferguson et al., 2007; Hayashi et al., 2008).

Compared to dynamin 1 single KO synapses, dynamin 1, 3 DKO synapses revealed a more severe endocytic defect, as shown in Fig. 5A and B by the more clustered immunoreactivity of the clathrin adaptor AP-2 (antibodies directed against its α-adaptin subunit). A corresponding clustering was observed for other presynaptically enriched endocytic proteins such as clathrin, amphiphysin 1 and epsin 1, while staining for a postsynaptic marker (PSD95) did not show any change (Fig. 5C). Furthermore, this phenotype became detectable earlier during the differentiation of DKO neuronal cultures relative to dynamin 1 single KO cultures (Fig. S5A and B), which is consistent with a lowering of the threshold at which the endocytic capacity of the DKO cells cannot keep up with the level of neuronal activity and synaptic vesicle exocytosis. Importantly, such clustering occurred at both excitatory and at inhibitory presynaptic terminals, as revealed by counterstaining for vGLUT1 and VGAT, synaptic vesicle neurotransmitter transporters at glutamatergic and GABAergic synapses respectively (Fig. 5D).

Massive accumulation of endocytic clathrin coated pits and loss of synaptic vesicles

This phenotype and the morphology of the endocytic intermediates in DKO neurons was further investigated by electron microscopy and electron tomography. The ultrastructure of DKO synapses strongly indicated a major presynaptic endocytic defect, with a very high abundance (but with variability from synapse to synapse) of clathrin coated vesicular profiles in the same size range of synaptic vesicles (Fig.6 A-F). In sections of some nerve terminals, synaptic vesicles had been almost completely, or even completely, replaced by up to hundreds of clathrin coated structures (Fig. 6E and H), although, surprisingly, some normal-looking DKO nerve terminals [abundant presence of synaptic vesicles and few

endocytic intermediates] were observed (Fig. 6B and F). In presynaptic terminals of DKO neurons, the diameter of synaptic vesicles was on average larger and more heterogeneous **(**Fig. S6A**)** which may contribute to the increase in charge transfer detected for mEPSPs (Fig. 3E). Interestingly there was a correlation between increased synaptic vesicle diameter and the degree to which synaptic vesicles were depleted in a given nerve terminal (Fig. S6B), suggesting that in these terminals the fidelity of the synaptic vesicle reformation process was more severely compromised. The accessibility of the endocytic structures in DKO nerve terminals to extracellular tracer (CTX-HRP under ice- cold conditions, Fig. 6G) and direct observation of electron tomography reconstructions (Fig. 6H-J) supported the interpretation that they were coated pits that had not undergone fission from the plasma membrane.

Tomographic reconstruction from multiple serial sections further demonstrated a very peculiar organization of the endocytic intermediates (Fig. 6I-L). The overwhelming majority of the pits originated from a limited number of long invaginations of the plasma membrane (see Fig. 6 H, K and L for examples), which in turn were connected to the outer surface of the terminal by narrow necks (22.7+/−4.8 nm, N=12, Fig. S5F). Overall, these endocytic intermediates resembled those observed in some dynamin 1 KO synapses (Ferguson et al., 2007; Hayashi et al., 2008), although their abundance, and the corresponding depletion of synaptic vesicles, was on average greater at DKO synapses.

While the clathrin coated pits accumulating in the DKO had a size similar to that of synaptic vesicles, they were less densely packed than synaptic vesicles (Fig. 6B versus C). Furthermore, the overall loss of synaptic vesicles was not fully accounted for by the increase in clathrin coated pits (Fig. 6F), suggesting that synaptic vesicle membranes might be partially trapped within the axonal plasma membrane outside of pits. Such a possibility agrees with the increased steady-state plasma membrane abundance of the vGlut1-pHlourin reporter in DKO neurons (Fig. 4A). As a result, immunofluorescence for intrinsic membrane proteins of synaptic vesicles (synaptophysin, synaptobrevin, synaptotagmin and SV2), which are expected to be enriched in these pits, was less punctate in DKO nerve terminals than in control nerve terminals where the puncta correspond to abundant and highly clustered synaptic vesicles (Fig. 7A and not shown). However, not surprisingly, given the loss of synaptic vesicles, the most striking change was observed for synapsin 1 and Rab3a, two peripheral proteins of synaptic vesicles (De Camilli et al., 1990; Fischer von Mollard et al., 1990) that dissociate from the vesicle prior to, or in parallel with, exocytosis and then re-associate with newly reformed synaptic vesicles once the endocytic /recycling journey is completed (Chi et al., 2001; Giovedi et al., 2004; Star et al., 2005). Immunoreactivities for these proteins lost their normally highly punctate enrichment within presynaptic terminals and became more diffusely spread out along the axonal length (Fig. 7A). Biochemical analysis of the subcellular localization of synaptic vesicle proteins (synaptotagmin 1 and synaptophysin) by a cell surface biotinylation based strategy confirmed an increase in their plasma membrane levels (Fig. 7B).

The accumulation of clathrin coated intermediates is activity-dependent and reversible

The ultrastructural changes of many DKO nerve terminals described above (Fig. 6) revealed a near complete switch from a “secretion-ready mode” to an “endocytic mode”, where the large clusters of synaptic vesicles, which represent the defining morphological feature of synapses, are replaced by a massive accumulation of clathrin coated pits. We asked whether these dramatic changes are reversible upon silencing of electrical activity (Ferguson et al., 2007). Neurons were first allowed to differentiate over 14 days in culture so that they would exhibit a strong accumulation of endocytic intermediates, and then exposed to tetrodotoxin (TTX, 1μM, overnight) to silence neuronal network activity. Following TTX treatment, immunofluorescence for α-adaptin (and other clathrin coat components) became diffuse

(Fig. 8 A-C) and electron microscopy showed a reduction of clathrin coated pit number (Fig. 8 D-F). This reversal of the endocytic phenotype was accompanied by a recovery of synaptic vesicle pools as judged by electron microscopy observations and by the clustering of synapsin 1 (Fig. 8A-F). It was further accompanied by an increase in EPSC amplitude from 0.36 +/− 0.11 nA in DKO cultures kept in normal medium compared to 0.92 +/− 0.74 nA, (t test, $p<0.05$) in cultures exposed to TTX overnight.

In a minor subset of processes, where the clustering of immunoreactivity for clathrin coat components was very intense and seemed to fill the entire process, such immunoreactivity did not disperse after TTX treatment (Fig. S5C). These processes were identified as axons, because of their emergence from stalks positive for ankyrin G, a marker of axon initial segments (Fig. S5D). They were further identified as axons of GABAergic neurons because of their reactivity with antibodies directed against VGAT, a marker of GABA containing synaptic vesicles (Fig. S5E). More specifically, they occur in the subset of parvalbumin-positive GABAergic interneurons neurons (Fig. S5F), a neuronal population that is characterized by high rates of activity (Bartos et al., 2007). We speculate that in such neurons the accumulation of endocytic intermediates may have been particularly strong due to their high basal level of synaptic activity, and thus irreversible, eventually leading to death (Garcia-Junco-Clemente et al., 2010; Luthi et al., 2001). This could explain the overall lower levels of parvalbumin, GAD and VGAT in DKO cultures (Fig. 2E). We conclude that the heterogeneous ultrastructural changes observed at synapses of DKO neurons, i.e. ranging from massive replacement of synaptic vesicles by coated pits at many nerve terminals to nearly normal morphology at other nerve terminals, is likely to reflect differences in functional state/activity levels, rather than different mechanisms of synaptic vesicle reformation in a subset of neurons.

Enhanced synapsin phosphorylation in spite of decreased network activity

Binding of synapsin 1 to the synaptic vesicle membrane is regulated by phosphorylation of its tail region (Jovanovic et al., 2001). Upon nerve terminal stimulation, the CamKII dependent phosphorylation of sites 2 and 3 in this region produces a shift of the protein from a clustered distribution on synaptic vesicles to a diffuse cytosolic distribution in axons (Chi et al., 2003). The less efficient synaptic transmission observed in DKO cultures relative to controls (Fig. 3) suggested lower levels of global network activity observed in DKO cultures and thus predicted a lower phosphorylation state of these sites as well as a general decrease of biochemical parameters that report activity. Indeed, we observed a striking decrease in the levels of the immediate early gene Arc/Arg3.1 (Tzingounis and Nicoll, 2006) and of phospho-CREB (Ser133, Fig. 8G) (Sheng et al., 1991). Surprisingly, however, an antibody specifically directed against phosphorylated sites 2 and 3 of synapsin 1 revealed a stronger signal in DKO cultures (Fig. 8 G and H). Since the accumulation of synaptic vesicle membranes in an endocytic state (clathrin coated pits) in DKO cells clearly makes vesicle membranes unavailable for synapsin binding, this finding reveals the occurrence of mechanisms to coordinate the phosphorylation state of synapsin with progression of the synaptic vesicle cycle. In support of this interpretation, the recovery of synaptic vesicle numbers following treatment with TTX (Fig. 8E) is accompanied by a reduction of synapsin 1 site 2,3 phosphorylation in the DKO neurons (Fig. 8 I and J).

Discussion

We have used biochemical, electrophysiological, genetic and microscopy tools to elucidate the function of dynamin isoforms in synaptic transmission. Our studies demonstrate a major function for dynamin 3 presynaptically that overlaps and synergizes with that of dynamin 1. However, while absence of dynamin 3 worsens the phenotype produced by the loss of dynamin 1, both at the organismal and synaptic levels, nervous system development is not

grossly affected by the lack of both isoforms. Neurons lacking both dynamins develop, differentiate and establish synapses in vitro. Most strikingly, nerve terminals can recycle synaptic vesicles in their absence implying that dynamin 2 alone and/or dynamin-independent mechanisms are sufficient to support basic synaptic function. These results collectively demonstrate that neither dynamin 1 nor 3 are essential for regenerating synaptic vesicles, but rather contribute to the efficiency of this process.

The overlapping function of dynamin 1 and 3 in nerve terminals is supported by their similar localizations and interactions and by the more striking structural and functional defects of the presynapse observed in dynamin 1, 3 DKO neurons relative to dynamin 1 KO neurons. Furthermore, the neonatal lethal phenotype of the DKO far exceeded the severity of the dynamin 1 single KO phenotype (Ferguson et al., 2007) in spite of the lack of an obvious phenotype in dynamin 3 KO mice. While this genetic interaction could conceivably arise due to multiple mechanisms, our data suggests a synergistic function of dynamin 1 and 3 in synaptic vesicle endocytosis. This interpretation is further supported by the strong enrichment of dynamin 3 at presynaptic terminals of dynamin 1 KO neurons (Ferguson et al, 2007). Unique functions of dynamin 1 and 3 relative to dynamin 2 likely exist, including differential interactions with other proteins and perhaps phosphorylation-based regulatory mechanisms, but these functions are not essential for the basic mechanism of synaptic vesicle endocytosis.

A selective enrichment of dynamin 3 in dendritic spines was reported previously (Gray et al., 2003; Lu et al., 2007). However, we have shown here that the signal produced by the dynamin 3 antibody used in those studies is not abolished in dynamin 3 KO neurons (Fig. 1E). In an additional observation relating to evaluation and validation of anti-dynamin antibody specificity in our KO mice, we observed that the prominent presynaptic immunoreactivity recognized by the widely used Hudy 1 antibody (Warnock et al., 1995), that is typically thought to reflect dynamin 1 (Takei et al., 1995), was not abolished in dynamin 1 KO neurons (Fig. S1A and B). Importantly, although our results demonstrate a major function of dynamin 3 presynaptically, they do not speak against a likely function for both dynamin 3 and dynamin 1 in clathrin mediated endocytosis that takes place in other neuronal sub-compartments including post-synaptically but which are beyond the scope of the present study.

While a dramatic accumulation of clathrin coated pits was observed at a subset of DKO synapses, these intermediates converted to synaptic vesicles in the majority of neurons within hours upon silencing of neuronal activity (Fig. 8 A-F). Furthermore, endocytic recovery from stimulation-evoked exocytosis was still observed, albeit at a slower rate, in DKO neurons (Fig. 4). Thus, the critical contributions of dynamin 1 and 3 to the recycling of synaptic vesicles do not seem to reflect a unique and specific function of these two dynamins. A simple interpretation of our results is that dynamin 2, which is expressed in neurons at a much lower concentration than the combined concentration of dynamin 1 and dynamin 3, yet at a concentration that is in the same range of that of dynamin 2 in non-neuronal cells (Ferguson et al., 2007), can support a low rate of synaptic vesicle endocytosis in addition to house-keeping forms of clathrin mediated endocytosis. A contribution of dynamin 2 to synaptic vesicle recycling is supported by the partial ability of this isoform to rescue the dynamin 1 KO phenotype when it is over-expressed (Ferguson et al., 2007).

The potential existence of a dynamin-independent pathway for synaptic vesicle reformation also warrants consideration and is supported by reports that a much limited form of synaptic transmission persists after manipulations expected to perturb dynamin function, such as microinjection of GTPγS or peptides (Xu et al, 2008; Shupliakov et al, 1997; Sundborger et al, 2011). Furthermore, studies with dynasore, an inhibitor of dynamin GTPase activity,

have demonstrated a complete block of the compensatory synaptic vesicle internalization that follows after triggered exocytosis (Newton et al., 2006) but synaptic vesicle endocytosis still occurred under conditions of spontaneous release (Chung et al, 2010). Dynasore only inhibits dynamin's GTPase activity by ~80%, based on biochemical studies (Macia et al., 2006; Chung et al, 2010) thus sparing ~20% activity, an amount that is more than the percent of total dynamin acounted for by dynamin 2 in neurons (Fig. 2B). The high efficacy of dynasore in some studies, in spite of its incomplete inhibition of dynamin, suggests a dominant-negative effect of dynasore-bound dynamin or an off-target effect of the drug.

Studies of dynamin 1 KO neurons revealed that the strong presynaptic endocytic phenotype was predominantly restricted to GABAergic synapses under conditions of spontaneous network activity (Hayashi et al., 2008). This selective phenotype was proposed to arise from a higher rate of tonic activity at such synapses. However, in dynamin 1, 3 DKO neurons, clathrin coated pits accumulated robustly at both excitatory and inhibitory synapses. We suggest that the combined loss of dynamin 1 and 3 lowers the endocytic capacity to a point where it can no longer keep pace with the spontaneous network activity level even in excitatory neurons. We further suspect that an initial loss of inhibition, due to selective vulnerability of GABAergic interneurons, could disinhibit network activity within the DKO cultures resulting in excitatory neurons that drive themselves to the point of exhaustion. Importantly, there was evidence for a greater sensitivity of parvalbumin-positive GABAergic neurons, as indicated by a stronger and irreversible endocytic phenotype. This observation may reflect a more general vulnerability of this subpopulation of GABAergic interneurons as their high activity levels have been proposed to confer added sensitivity to another genetic perturbation (Garcia-Junco-Clemente et al., 2010). Furthermore, a spontaneous dynamin 1 missense mutation in mice was recently reported that is permissive for development but which confers seizure susceptibility that could arise from greater sensitivity of GABAergic interneurons to endocytic perturbation (Boumil et al, 2010).

Interestingly, in spite of the strong decrease in average EPSC amplitude, the frequency and amplitude of mEPSCs was not markedly affected in DKO cultures (Fig. 3). Perhaps, under conditions where efficiency of recycling is severely impaired, newly formed vesicles are rapidly made available for spontaneous release and even the very low levels of dynamin 2 or dynamin-independent mechanisms may be adequate to replenish vesicles consumed by the more modest rates of spontaneous release. These considerations fit with the previous report that spontaneous transmission was relatively spared following treatment of cultured neurons with dynasore (Chung et al, 2010).

The morphology of the endocytic intermediates that accumulate in DKO nerve terminals provides new insight into the mechanisms acting upstream of dynamin in endocytosis and, more generally, in the cell biology of nerve terminals. Like in fibroblasts that lack dynamin (Ferguson et al., 2009), the ability of clathrin coated pits to mature to a very advanced state with narrow necks argues against essential functions for dynamin earlier in the process. Coated pits of dynamin 1, 3 mutant nerve terminals, however, are quite different from those observed in fibroblasts with no dynamin: 1) They are considerably smaller and highly homogeneous in diameter, consistent with their being direct precursors of synaptic vesicles. Thus, factors other than neuron-specific dynamin isoforms or high dynamin abundance must impose this small curvature. 2) Their narrow necks, while constricted and elongated, are shorter than the narrow long stalks of arrested fibroblastic clathrin coated pits. Considering that actin polymerization was shown to be required for the formation of the long necks in non-neuronal cells (Ferguson et al., 2009), it is of interest that clathrin mediated endocytosis of synaptic vesicles was reported not to be dependent on actin (Sankaranarayanan et al., 2003). 3) Clathrin coated pits of DKO nerve terminals typically originate from deep invaginations of the plasma membrane that are often decorated by numerous, sometimes

100's of such pits. Each such tubular invagination is connected to the outer plasma membrane by a narrow constriction similar to the neck of clathrin coated pits (Fig. S6G and H). This structural arrangement allows for accommodation of the vast increase in plasma membrane area produced by massive synaptic vesicle exocytosis without expanding the outer surface of the presynaptic terminal.

The great abundance of clathrin coated pits emphasizes the importance of fission as a trigger to uncoating. This is consistent with the report that auxilin, a critical co-factor for clathrin uncoating (Yim et al., 2010), is most strongly recruited to pits only after fission (Massol et al., 2006). Accordingly, while immunoreactivity for a variety of major endocytic clathrin coat components analyzed (light chain of clathrin, AP-2, AP180, epsin) was clustered in DKO nerve terminals, auxilin, which is an abundant component of purified brain clathrin coated vesicles (Ahle and Ungewickell, 1990), was not (Fig. 5D). These findings fit with a model in which i) endocytic clathrin coated pits can assemble only at the $PI(4,5)P_2$ rich plasma membrane, ii) fission is coupled to $PI(4,5)P_2$ dephosphorylation, iii) modification of the lipid composition of the membrane triggers uncoating by promoting adaptor dissociation and auxilin/Hsc70 recruitment (Cremona et al, 1999; Massol et al, 2006; Yim et al, 2010; Guan et al., 2010).

Overall, our findings reveal a remarkable plasticity of nerve terminals. In a subset of dynamin 1,3 DKO neurons, spontaneous network activity resulted in a nearly complete shift from the typical "secretion-ready state" (abundance of synaptic vesicles clustered at active zones) to an "endocytic state" in which the great majority, possibly all, synaptic vesicles were replaced by clathrin coated pits. This shift implies a cross-talk between the cytosol and the membranes because proteins peripherally associated with the cytosolic face of synaptic vesicles, such as synapsin and Rab3, must be replaced, in a reversible fashion, with proteins of the clathrin coats and other endocytic factors. The different lipid environment (phosphoinositides and possibly other phospholipids) that surrounds synaptic vesicle proteins as they cycle between vesicles and the plasma membrane likely plays a role in these changes (Di Paolo and De Camilli, 2006). However, the enhancement of the phosphorylation state of synapsin at sites 2 and 3 when nerve terminals are in an endocytic state, in spite of a global decrease in activity-dependent parameters, suggests the additional occurrence of feed-back mechanisms between the progression of synaptic vesicle membranes along their exo-endocytic cycle and signaling pathways within nerve terminals. Elucidating the mechanisms underlying this link will be an interesting focus of future work.

Conclusions

In summary, contrary to models where the major functions of individual dynamin isoforms are distinct from one another, our results support an overall conservation of such functions, so that each isoform can at least partially replace the other. Clearly, unique roles of the three dynamins and of their splice variants could act to fine-tune the efficiency and regulation of synaptic vesicle recycling and of other endocytic reactions. However, the most important parameter that defines the collective contributions of dynamin 1 and 3 to the rapid reformation of synaptic vesicles after endocytosis is their abundance in neurons and nerve terminals. Neither protein is required for synaptic vesicle reformation, but their presence and overall abundance account for the impressive efficiency of synaptic vesicle endocytosis that is critical for sustaining normal synaptic transmission.

Experimental procedures

A complete description of experimental procedures is provided as Supplemental Data.

Gene Targeting Strategies

The dynamin 3 conditional KO targeting strategy (Fig. S1D) resulted in the flanking of a 1.8 kb region containing exon 2 with loxP sites. Mating to a Cre deleter strain (Lewandoski et al., 1997) yielded the dynamin 3 KO allele. The KO allele of dynamin 1 used in this study was previously described (Ferguson et al., 2007; Ferguson et al., 2009). Animal care and use was carried out in accordance with our institutional guidelines.

Antibodies

Antibodies and their sources are provided in the supplemental material.

Biochemical Methods

For GST pulldowns, fusion proteins comprising the core, conserved PRD regions of mouse dynamin 1 (amino acids 747-852), dynamin 2 (amino acids 741-845) and dynamin 3 (amino acids 741-838) were prepared and isolated by standard methods from E. coli [BL21(DE3)-RIPL] and used to enrich for known binding partners from 1% TX-100 extracts of mouse brain tissue (Slepnev et al., 1998).

For immunoblotting, cortical neurons at 14-21 DIV were rinsed in Tyrode's buffer and lysed in 150 mM NaCl, 2 mM EDTA, 50 mM Tris-HCl pH 7.4 with 1% SDS. Total cell lysates were loaded on SDS-PAGE gels, transferred to nitrocellulose and immunoblotted with the specified primary antibodies. HRP and IRDye conjugated secondary antibodies were used for chemiluminescent and infrared imaging (Odyssey, LI-COR) respectively. Cell surface biotinylation methods were described previously (Ferguson et al., 2009).

Primary Cortical Neuron Cultures

Primary cortical neurons were prepared from P0 neonatal mouse brains by previously described methods (Ferguson et al., 2007).

Immunofluorescence

Cortical neurons were fixed with 4% paraformaldehyde, 4% sucrose in 0.12 M sodium phosphate buffer. For brain sections, mice were perfused transcardially with 4% paraformaldehyde in 0.1 M phosphate buffer. Preparation of frozen sections and immunofluorescence were performed by standard procedures.

Electron Microscopy

Primary cortical neurons were fixed with 1.3% glutaraldehyde in 66 mM sodium cacodylate buffer, post-fixed in 1% OsO_4, 1.5% $K_4Fe(CN)_6$, 0.1M sodium cacodylate, stained with 0.5% uranyl magnesium acetate, dehydrated and embedded in Embed 812 (E.M.S., Hatfield, PA). Diaphragms and brain tissue of P0 mice were fixed by immersion in 2% paraformaldehyde, 2% glutaraldehyde in 0.1M cacodylate buffer ph 7.4. Additional transmission electron microscopy and tomography were performed as previously described (Ferguson et al., 2007; Hayashi et al., 2008).

Functional Studies

For electrophysiology, cortical neurons were plated at a density of 75000/cm^2 and recorded at room temperature (20-22 °C) between 10-14 DIV.

For dynamic imaging studies of exo-endocytosis, vGlut1-pHluorin was transfected into cortical neurons 8 days after plating and imaging was performed 13-25 days after plating.

Statistical Analysis

Statistical significance was determined using t tests or ANOVA followed by Tukey's post hoc test and data with p values <0.05 are indicated by an asterisk(*).

Supplementary Material

Refer to Web version on PubMed Central for supplementary material.

Acknowledgments

We thank Frank Wilson, Lijuan Liu, Louise Lucast, Livia Tomasini, Kumi Mesaki and Ricky Kwan for superb technical assistance. We appreciate the contributions of Tim Nottoli (Yale Cancer Center Animal Genomics Shared Resource) towards gene targeting and the support of the Yale Center for Genomics and Proteomics. This work was supported in part by the G. Harold and Leila Y. Mathers Charitable Foundation, National Institutes of Health grants (R37NS036251, DK45735 and DA018343), the W.M. Keck Foundation and a NARSAD distinguished Investigator Award to P.D.C., a pilot grant from the Yale DERC to X.L., Grant RR-000592 from the National Center for Research Resources of the National Institutes of Health to J.R. McIntosh, National Institutes of Health grant NS36942 to T.A.R. and a Canadian Institutes of Health Research fellowship to S.M.F..

References

Ahle S, Ungewickell E. Auxilin, a newly identified clathrin-associated protein in coated vesicles from bovine brain. J Cell Biol. 1990; 111:19–29. [PubMed: 1973169]

Anggono V, Robinson PJ. Syndapin I and endophilin I bind overlapping proline-rich regions of dynamin I: role in synaptic vesicle endocytosis. J Neurochem. 2007; 102:931–943. [PubMed: 17437541]

Anggono V, Smillie KJ, Graham ME, Valova VA, Cousin MA, Robinson PJ. Syndapin I is the phosphorylation-regulated dynamin I partner in synaptic vesicle endocytosis. Nat Neurosci. 2006; 9:752–760. [PubMed: 16648848]

Aramburu J, Yaffe MB, Lopez-Rodriguez C, Cantley LC, Hogan PG, Rao A. Affinity-driven peptide selection of an NFAT inhibitor more selective than cyclosporin A. Science. 1999; 285:2129–2133. [PubMed: 10497131]

Balaji J, Ryan TA. Single-vesicle imaging reveals that synaptic vesicle exocytosis and endocytosis are coupled by a single stochastic mode. Proc Natl Acad Sci U S A. 2007; 104:20576–20581. [PubMed: 18077369]

Bartos M, Vida I, Jonas P. Synaptic mechanisms of synchronized gamma oscillations in inhibitory interneuron networks. Nat Rev Neurosci. 2007; 8:45–56. [PubMed: 17180162]

Blondeau F, Ritter B, Allaire PD, Wasiak S, Girard M, Hussain NK, Angers A, Legendre-Guillemin V, Roy L, Boismenu D, et al. Tandem MS analysis of brain clathrin-coated vesicles reveals their critical involvement in synaptic vesicle recycling. Proc Natl Acad Sci U S A. 2004; 101:3833–3838. [PubMed: 15007177]

Boumil RM, Letts VA, Roberts MC, Lenz C, Mahaffey CL, Zhang ZW, Moser T, Frankel WN. A missense mutation in a highly conserved alternate exon of dynamin-1 causes epilepsy in fitful mice. PLoS Genet. 2010; 6

Cao H, Garcia F, McNiven MA. Differential distribution of dynamin isoforms in mammalian cells. Mol Biol Cell. 1998; 9:2595–2609. [PubMed: 9725914]

Carroll RC, Beattie EC, Xia H, Luscher C, Altschuler Y, Nicoll RA, Malenka RC, von Zastrow M. Dynamin-dependent endocytosis of ionotropic glutamate receptors. Proc Natl Acad Sci U S A. 1999; 96:14112–14117. [PubMed: 10570207]

Chi P, Greengard P, Ryan TA. Synapsin dispersion and reclustering during synaptic activity. Nat Neurosci. 2001; 4:1187–1193. [PubMed: 11685225]

Chi P, Greengard P, Ryan TA. Synaptic vesicle mobilization is regulated by distinct synapsin I phosphorylation pathways at different frequencies. Neuron. 2003; 38:69–78. [PubMed: 12691665]

Chowdhury S, Shepherd JD, Okuno H, Lyford G, Petralia RS, Plath N, Kuhl D, Huganir RL, Worley PF. Arc/Arg3.1 interacts with the endocytic machinery to regulate AMPA receptor trafficking. Neuron. 2006; 52:445–459. [PubMed: 17088211]

Chung C, Barylko B, Leitz J, Liu X, Kavalali ET. Acute dynamin inhibition dissects synaptic vesicle recycling pathways that drive spontaneous and evoked neurotransmission. The Journal of Neuroscience. 2010; 30:1363–1376. [PubMed: 20107062]

Conner SD, Schmid SL. Regulated portals of entry into the cell. Nature. 2003; 422:37–44. [PubMed: 12621426]

De Camilli P, Benfenati F, Valtorta F, Greengard P. The synapsins. Annu Rev Cell Biol. 1990; 6:433–460. [PubMed: 1980418]

Di Paolo G, De Camilli P. Phosphoinositides in cell regulation and membrane dynamics. Nature. 2006; 443:651–657. [PubMed: 17035995]

Dittman J, Ryan TA. Molecular circuitry of endocytosis at nerve terminals. Annu Rev Cell Dev Biol. 2009; 25:133–160. [PubMed: 19575674]

Doherty GJ, McMahon HT. Mechanisms of endocytosis. Annu Rev Biochem. 2009; 78:857–902. [PubMed: 19317650]

Ferguson SM, Brasnjo G, Hayashi M, Wolfel M, Collesi C, Giovedi S, Raimondi A, Gong LW, Ariel P, Paradise S, et al. A selective activity-dependent requirement for dynamin 1 in synaptic vesicle endocytosis. Science. 2007; 316:570–574. [PubMed: 17463283]

Ferguson SM, Raimondi A, Paradise S, Shen H, Mesaki K, Ferguson A, Destaing O, Ko G, Takasaki J, Cremona O, et al. Coordinated actions of actin and BAR proteins upstream of dynamin at endocytic clathrin-coated pits. Dev Cell. 2009; 17:811–822. [PubMed: 20059951]

Fischer von Mollard G, Mignery GA, Baumert M, Perin MS, Hanson TJ, Burger PM, Jahn R, Sudhof TC. rab3 is a small GTP-binding protein exclusively localized to synaptic vesicles. Proc Natl Acad Sci U S A. 1990; 87:1988–1992. [PubMed: 2155429]

Garcia-Junco-Clemente P, Cantero G, Gomez-Sanchez L, Linares-Clemente P, Martinez-Lopez JA, Lujan R, Fernandez-Chacon R. Cysteine string protein-alpha prevents activity-dependent degeneration in GABAergic synapses. The Journal of neuroscience : the official journal of the Society for Neuroscience. 2010; 30:7377–7391. [PubMed: 20505105]

Giovedi S, Darchen F, Valtorta F, Greengard P, Benfenati F. Synapsin is a novel Rab3 effector protein on small synaptic vesicles. II. Functional effects of the Rab3A-synapsin I interaction. J Biol Chem. 2004; 279:43769–43779. [PubMed: 15265868]

Granseth B, Odermatt B, Royle SJ, Lagnado L. Clathrin-mediated endocytosis is the dominant mechanism of vesicle retrieval at hippocampal synapses. Neuron. 2006; 51:773–786. [PubMed: 16982422]

Gray NW, Fourgeaud L, Huang B, Chen J, Cao H, Oswald BJ, Hemar A, McNiven MA. Dynamin 3 is a component of the postsynapse, where it interacts with mGluR5 and Homer. Curr Biol. 2003; 13:510–515. [PubMed: 12646135]

Guan R, Han D, Harrison SC, Kirchhausen T. Structure of the PTEN-like region of auxilin, a detector of clathrin-coated vesicle budding. Structure. 2010; 18:1191–1198. [PubMed: 20826345]

Hayashi M, Raimondi A, O'Toole E, Paradise S, Collesi C, Cremona O, Ferguson SM, De Camilli P. Cell- and stimulus-dependent heterogeneity of synaptic vesicle endocytic recycling mechanisms revealed by studies of dynamin 1-null neurons. Proc Natl Acad Sci U S A. 2008; 105:2175–2180. [PubMed: 18250322]

Hirst J, Robinson MS. Clathrin and adaptors. Biochim Biophys Acta. 1998; 1404:173–193. [PubMed: 9714795]

Jovanovic JN, Sihra TS, Nairn AC, Hemmings HC Jr. Greengard P, Czernik AJ. Opposing changes in phosphorylation of specific sites in synapsin I during Ca2+-dependent glutamate release in isolated nerve terminals. J Neurosci. 2001; 21:7944–7953. [PubMed: 11588168]

Jung N, Haucke V. Clathrin-Mediated Endocytosis at Synapses. Traffic. 2007; 8:1129–1136. [PubMed: 17547698]

Lai MM, Hong JJ, Ruggiero AM, Burnett PE, Slepnev VI, De Camilli P, Snyder SH. The calcineurin-dynamin 1 complex as a calcium sensor for synaptic vesicle endocytosis. J Biol Chem. 1999; 274:25963–25966. [PubMed: 10473536]

Larsen MR, Graham ME, Robinson PJ, Roepstorff P. Improved detection of hydrophilic phosphopeptides using graphite powder microcolumns and mass spectrometry: evidence for in vivo doubly phosphorylated dynamin I and dynamin III. Mol Cell Proteomics. 2004; 3:456–465. [PubMed: 14762214]

Lewandoski M, Meyers EN, Martin GR. Analysis of Fgf8 gene function in vertebrate development. Cold Spring Harb Symp Quant Biol. 1997; 62:159–168. [PubMed: 9598348]

Lou X, Paradise S, Ferguson SM, De Camilli P. Selective saturation of slow endocytosis at a giant glutamatergic central synapse lacking dynamin 1. Proc Natl Acad Sci U S A. 2008; 105:17555–17560. [PubMed: 18987309]

Lu J, Helton TD, Blanpied TA, Racz B, Newpher TM, Weinberg RJ, Ehlers MD. Postsynaptic positioning of endocytic zones and AMPA receptor cycling by physical coupling of dynamin-3 to Homer. Neuron. 2007; 55:874–889. [PubMed: 17880892]

Luthi A, Di Paolo G, Cremona O, Daniell L, De Camilli P, McCormick DA. Synaptojanin 1 contributes to maintaining the stability of GABAergic transmission in primary cultures of cortical neurons. The Journal of neuroscience : the official journal of the Society for Neuroscience. 2001; 21:9101–9111. [PubMed: 11717343]

Macia E, Ehrlich M, Massol R, Boucrot E, Brunner C, Kirchhausen T. Dynasore, a cell-permeable inhibitor of dynamin. Dev Cell. 2006; 10:839–850. [PubMed: 16740485]

Massol R, Boll W, Griffin AM, Kirchhausen T. A burst of auxilin recruitment determines the onset of clathrin-coated vesicle uncoating. Proc Natl Acad Sci U S A. 2006 In Press.

Murthy VN, De Camilli P. Cell biology of the presynaptic terminal. Annu Rev Neurosci. 2003; 26:701–728. [PubMed: 14527272]

Newton AJ, Kirchhausen T, Murthy VN. Inhibition of dynamin completely blocks compensatory synaptic vesicle endocytosis. Proc Natl Acad Sci U S A. 2006; 103:17955–17960. [PubMed: 17093049]

Petrini EM, Lu J, Cognet L, Lounis B, Ehlers MD, Choquet D. Endocytic trafficking and recycling maintain a pool of mobile surface AMPA receptors required for synaptic potentiation. Neuron. 2009; 63:92–105. [PubMed: 19607795]

Praefcke GJ, McMahon HT. The dynamin superfamily: universal membrane tubulation and fission molecules? Nat Rev Mol Cell Biol. 2004; 5:133–147. [PubMed: 15040446]

Pucadyil TJ, Schmid SL. Conserved functions of membrane active GTPases in coated vesicle formation. Science. 2009; 325:1217–1220. [PubMed: 19729648]

Sankaranarayanan S, Atluri PP, Ryan TA. Actin has a molecular scaffolding, not propulsive, role in presynaptic function. Nat Neurosci. 2003; 6:127–135. [PubMed: 12536209]

Sankaranarayanan S, Ryan TA. Calcium accelerates endocytosis of vSNAREs at hippocampal synapses. Nat Neurosci. 2001; 4:129–136. [PubMed: 11175872]

Sheng M, Thompson MA, Greenberg ME. CREB: a Ca(2+)-regulated transcription factor phosphorylated by calmodulin-dependent kinases. Science. 1991; 252:1427–1430. [PubMed: 1646483]

Shepherd JD, Huganir RL. The cell biology of synaptic plasticity: AMPA receptor trafficking. Annu Rev Cell Dev Biol. 2007; 23:613–643. [PubMed: 17506699]

Shupliakov O, Low P, Grabs D, Gad H, Chen H, David C, Takei K, De Camilli P, Brodin L. Synaptic vesicle endocytosis impaired by disruption of dynamin-SH3 domain interactions. Science. 1997; 276:259–263. [PubMed: 9092476]

Slepnev VI, Ochoa GC, Butler MH, Grabs D, De Camilli P. Role of phosphorylation in regulation of the assembly of endocytic coat complexes. Science. 1998; 281:821–824. [PubMed: 9694653]

Stamm S, Casper D, Dinsmore J, Kaufmann CA, Brosius J, Helfman DM. Clathrin light chain B: gene structure and neuron-specific splicing. Nucleic Acids Res. 1992; 20:5097–5103. [PubMed: 1408826]

Star EN, Newton AJ, Murthy VN. Real-time imaging of Rab3a and Rab5a reveals differential roles in presynaptic function. J Physiol. 2005; 569:103–117. [PubMed: 16141272]

Sundborger A, Soderblom C, Vorontsova O, Evergren E, Hinshaw JE, Shupliakov O. An endophilin-dynamin complex promotes budding of clathrin-coated vesicles during synaptic vesicle recycling. J Cell Sci. 2011; 124:133–143. [PubMed: 21172823]

Takei K, McPherson PS, Schmid SL, De Camilli P. Tubular membrane invaginations coated by dynamin rings are induced by GTP-gamma S in nerve terminals. Nature. 1995; 374:186–190. [PubMed: 7877693]

Tebar F, Bohlander SK, Sorkin A. Clathrin assembly lymphoid myeloid leukemia (CALM) protein: localization in endocytic-coated pits, interactions with clathrin, and the impact of overexpression on clathrin-mediated traffic. Mol Biol Cell. 1999; 10:2687–2702. [PubMed: 10436022]

Tzingounis AV, Nicoll RA. Arc/Arg3.1: linking gene expression to synaptic plasticity and memory. Neuron. 2006; 52:403–407. [PubMed: 17088207]

Vaid KS, Guttman JA, Babyak N, Deng W, McNiven MA, Mochizuki N, Finlay BB, Vogl AW. The role of dynamin 3 in the testis. J Cell Physiol. 2007; 210:644–654. [PubMed: 17133358]

Warnock DE, Terlecky LJ, Schmid SL. Dynamin GTPase is stimulated by crosslinking through the C-terminal proline-rich domain. Embo J. 1995; 14:1322–1328. [PubMed: 7537212]

Xu J, McNeil B, Wu W, Nees D, Bai L, Wu LG. GTP-independent rapid and slow endocytosis at a central synapse. Nature neuroscience. 2008; 11:45–53.

Yim YI, Sun T, Wu LG, Raimondi A, De Camilli P, Eisenberg E, Greene LE. Endocytosis and clathrin-uncoating defects at synapses of auxilin knockout mice. Proc Natl Acad Sci U S A. 2010; 107:4412–4417. [PubMed: 20160091]

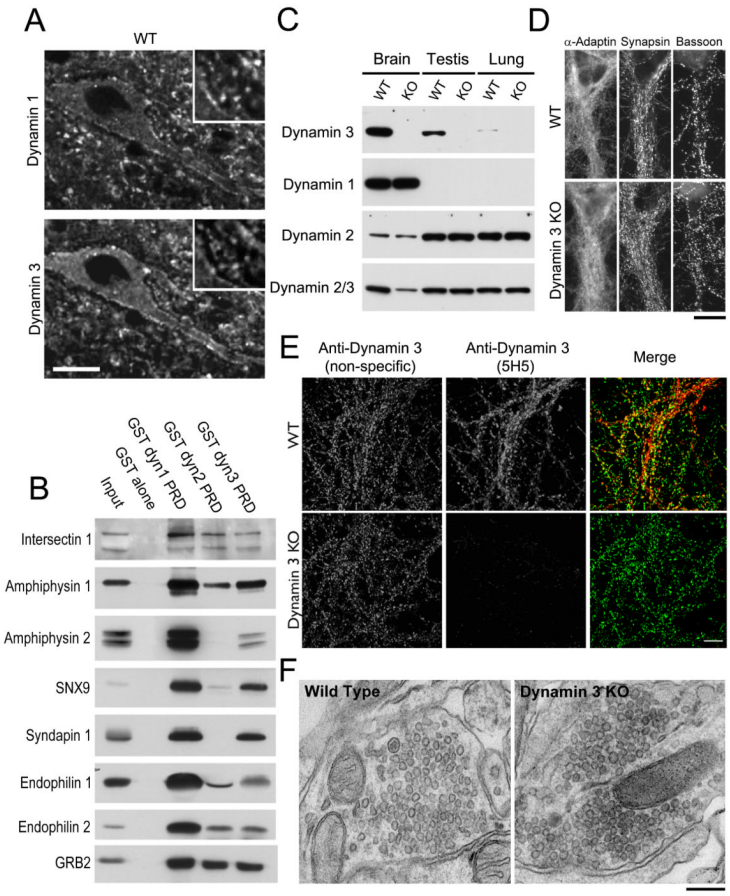

Figure 1.

Comparative analysis of dynamin 1 and 3 in the brain and generation of dynamin 3 KO mice. (**A**) Double immunofluorescence with isoform specific antibodies showing that dynamin 1 and 3 share a similar localization at synapses surrounding motor neurons (spinal cord ventral horn). (**B**) Evaluation of proteins binding to the proline rich domain (PRD) of dynamin 1, 2 and 3 by GST pulldown from mouse brain lysates followed by immunoblotting. (**C**) Immunoblot analysis of dynamin isoform levels in the indicated tissues in wild type and dynamin 3 KO mice. (**D**) Markers of clathrin coats (AP-2 subunit α-adaptin), synaptic vesicles (synapsin 1) and active zones (bassoon) do not show any change in localization in dynamin 3 KO cortical neurons in culture. (**E**) Loss of dynamin 3 immunofluorescence revealed by dynamin 3 specific antibodies (clone 5H5) in primary neuron cultures. A previously described anti-dynamin 3 antibody (Gray et al., 2003) generates a punctate, non-specific immunofluorescence of dendritic spines. (**F**) Electron micrographs of wildtype and dynamin 3 KO synapses respectively demonstrating presence of synaptic vesicles in synapses of both genotypes. Scale bars in A and E = 10μm, D = 20μm. Scale bar in E = 200 nm. See also Figure S1.

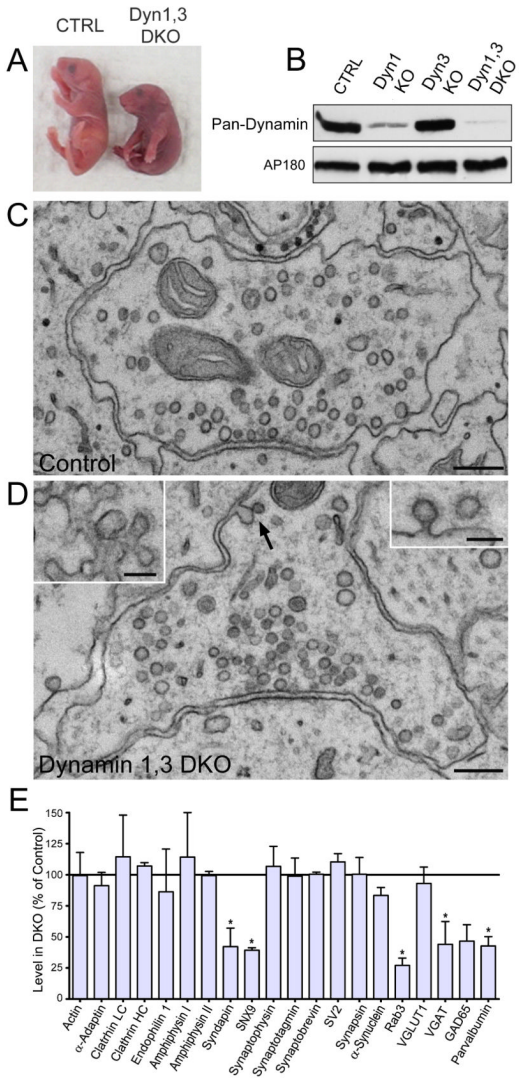

Figure 2.

Dynamin 1,3 DKO mice exhibit perinatal lethality. (**A**) Photograph of a control and a DKO littermate taken ~ 2 hours after birth. Note the cyanotic color, lack of milk in stomach and hunched posture of the DKO. (**B**) Immunoblotting of neuronal culture lysates derived from mice of the indicated genotypes with a pan-dynamin antibody. AP180 signal was used as a neuron specific endocytic protein loading control. (**C** and **D**) Electron micrographs of brainstem synapses from dynamin 3 KO and dynamin 1,3 DKO pups respectively. Note the presence of synaptic vesicles in the DKO but with some heterogeneity in synaptic vesicle size and clathrin coated endocytic intermediates (arrow and highlighted in the insets). (**E**) Summary of protein levels in control versus DKO cortical neuron cultures. Measurements were made from at least 3 independent pairs of samples (mean+/−SEM * $p<0.05$, t test). Scale bars in (C) and (D) = 150nm. See also Figure S2.

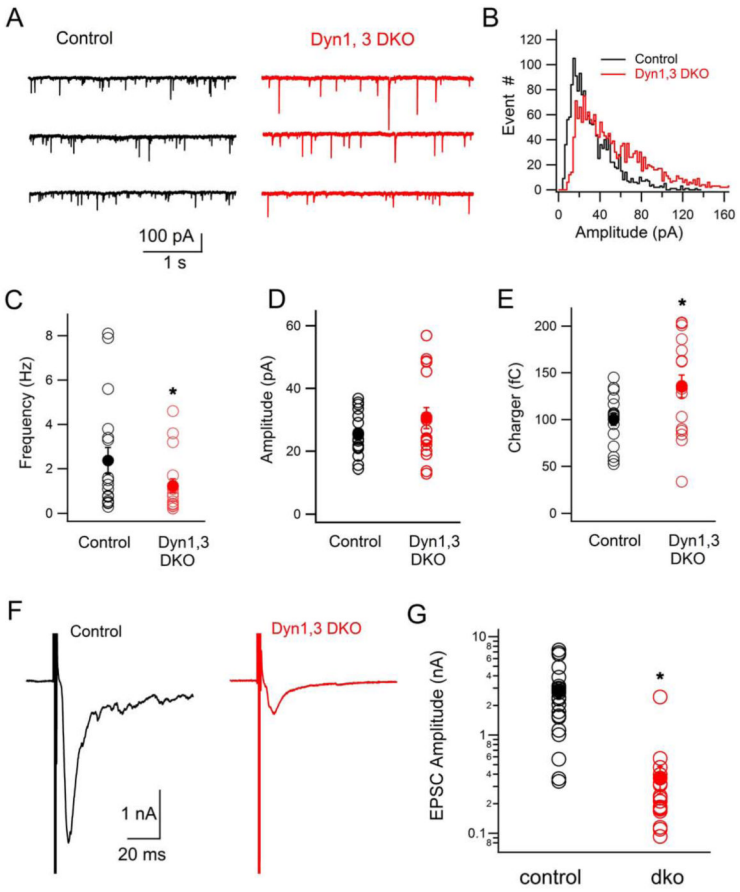

Figure 3.

Synaptic transmission at dynamin 1,3 DKO synapses. (**A**) Representative traces of mEPSCs from control (black) and DKO (red) neuronal cultures. (**B**) Amplitude distribution of mEPSCs (n=1547 and 1857 mEPSC events recorded from a selected control and DKO respectively as shown in **A**). (**C-E**) mEPSP frequency, peak amplitude and total charge transfer (averages from 18 control and 20 DKO neurons, $^{*}p<0.05$, t test). Open symbols show individual neurons and filled symbols show the average +/− SEM of each group. (**F**) Representative traces of evoked EPSCs from control and DKO neurons. (**G**) Summary of peak EPSC amplitudes plotted on a logarithmic scale (Control EPSC Amplitude: 2.82± 0.48 nA; DKO EPSC amplitude: 0.36±0.11nA, n=20 for each, t test $p<0.0001$). See also Figure S3

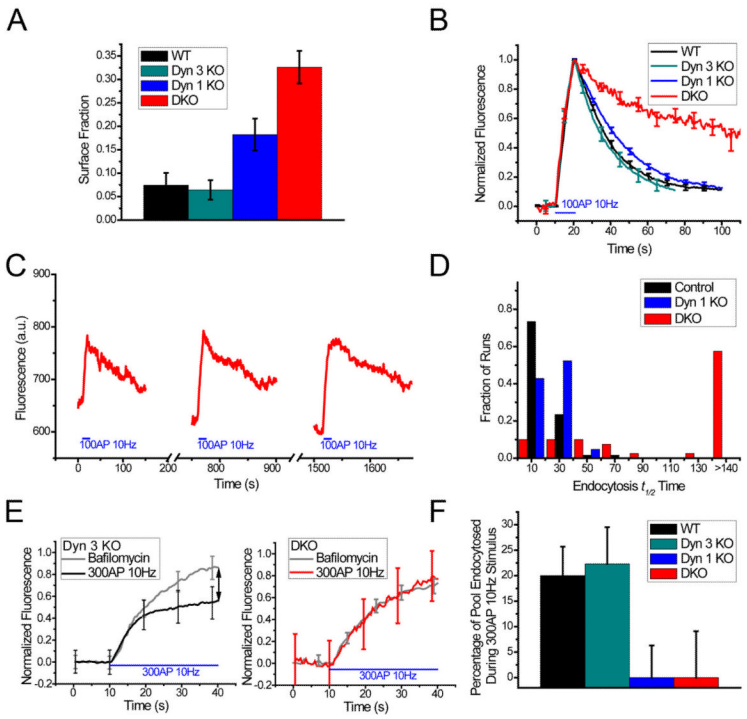

Figure 4.

Analysis of compensatory endocytosis. (**A**) Dynamin 1 KO and DKO cells have a greater fraction of the vGlut1-pHluorin stranded on the surface (p=0.02 and 0.001 versus WT or dynamin 3 KO littermates respectively, 2 sample t-test, N=11, 6, 10 and 2 for WT, dynamin 3 KO dynamin 1 KO and DKO respectively). (**B**) Averaged vGlut1-pHluorin responses to 100 AP stimulation at 10 Hz from wildtype (40 runs from 11 cells), dynamin 3 KO (22 runs from 6 cells), dynamin 1 KO (43 runs from 11 cells) and DKO (33 runs, 11 cells), see supplemental methods for error calculation. The deficit in the amount of vGlut1-pHluorin that was not endocytosed 40s after the end of the stimulus is significant for both the dynamin 1 KO as well as for the DKO ($p<0.05$ and $p=0.001$ respectively, two sample t test with dynamin 1 KO compared to WT littermates and DKO compared to dynamin 3 KO littermates). (**C**) Representative vGlut1-pHluorin trace of a DKO neuron responding to three consecutive rounds of stimulation (100AP at 10Hz) with 10 minutes recovery between stimulus challenges. Traces are averages from 28 regions of interest corresponding to individual presynaptic terminals of this neuron. $t_{1/2}$ times = 62s, 90s, >140s respectively. (**D**) Histogram of endocytosis $t_{1/2}$ times for control (pooled data from WT and dynamin 3 KO), dynamin 1 KO and DKOs in response to 100AP 10Hz stimulus. Runs which did not decay to half of the ΔF within the imaging window (140s), but recovered before the following run are binned into >140s. Controls: 64 runs from 18 cells, dynamin 1 KO: 40 runs from 11 cells, DKO: 40 runs from 12 cells. (**E**) Endocytosis occurring during stimulation was measured by the difference between a 300AP 10Hz train and after full recovery, a subsequent 10Hz train in the presence of the proton pump inhibitor bafilomycin. Data is normalized to the maximum fluorescence obtained during stimulation in the presence of bafilomycin. Such fluorescence represents the size of the recycling pool. The panel shows sample traces from a control (dynamin 3 KO) cell and a DKO cell that recover by endocytosis 32.0% and 0% respectively of the fluorescence increase produced by exocytosis during the stimulation interval. (**F**) Averages of the extent of endocytosis occurring during stimulation were 20+/−5.7% for WT, 24.6±4.8% for dynamin 3 KO, 0+/−6.3% for the dynamin 1 KO and 0±9.9% for DKOs from N=8, 5, 7 and 16 cells respectively. * p=0.006

for Dynamin 1 KO versus WT and p=0.03 for DKO versus dynamin 3 KO, (2 sample t-tests). Except where indicated otherwise in panel B, error bars represent the mean+/−SEM. See also Figure S4.

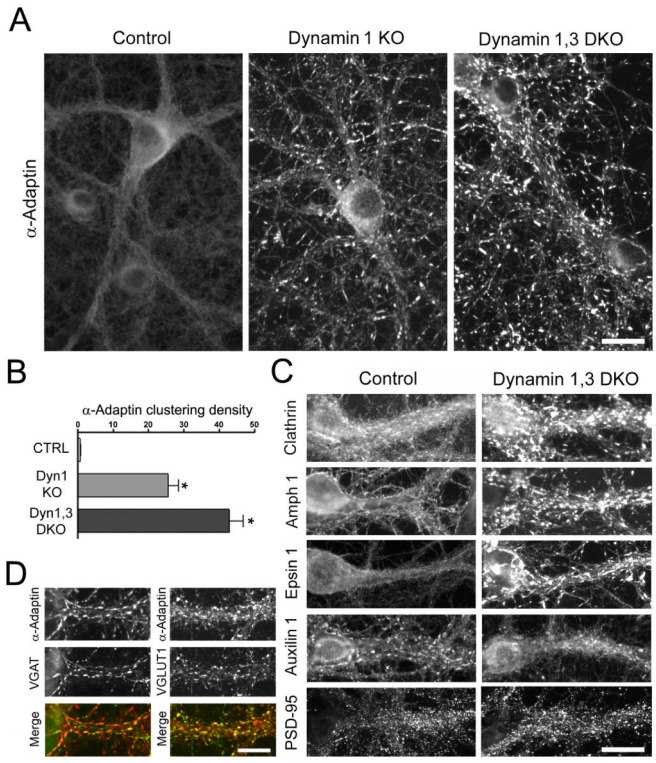

Figure 5.

Endocytic proteins accumulate at DKO presynaptic terminals. (**A**) α-adaptin immunofluorescence staining is more punctate in 18 DIV DKO neurons as compared to control or even to dynamin 1 single KO neurons (see an additional time point in Fig. S4). (**B**) Quantification of the abundance of presynaptic terminals showing intense α-adaptin clustering (mean+/−SEM, $^{*}p<0.001$ for Control versus Dyn 1 KO, Control versus DKO, and Dyn1 KO versus DKO, one way ANOVA with Tukey's post hoc test). (**C**) Double-labeling for α-adaptin and VGAT or vGLUT1 respectively. (**D**) Immunofluorescence analysis of protein localization in control versus DKO cultures (clathrin=clathrin light chain; Amph 1=amphiphysin 1). Scale bars = 20μm. See also Figure S5.

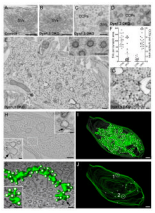

Figure 6.

Ultrastructural analysis of endocytic intermediates formed in the absence of dynamin 1 and 3. (**A**) Electron micrograph of a control presynaptic terminal filled with synaptic vesicles (SVs). (**B** and **C**) Examples of DKO presynaptic terminals that reflect the range in the severity of the phenotype from nearly normal (B) to a major accumulation of clathrin coated pits (CCPs) with few remaining synaptic vesicles (C). Clathrin coated pits can be recognized even at low magnification because of their less dense packing than synaptic vesicles. (**D**) Higher magnification view of interconnected clathrin coated pits at a DKO synapse. (**E**) Large nerve terminal entirely occupied by clathrin coated pits. Inset: High magnification view demonstrates the presence of a clathrin coat surrounding the budding pits. (**F**) Quantification of synaptic vesicle (left) and clathrin coated structure abundance (right) expressed as their number per synaptic profile (filled circles represent individual synapses, line and whiskers represent mean+/− SEM, $^{*}p<0.0001$, t test). (**G**) Accessibility to cholera toxin-HRP (during incubation on ice) supports the connectivity of endocytic structures (primarily clathrin coated pits) in DKO synapses to the extracellular space. (**H**) Tomographic section of a DKO synapse with a high number of endocytic clathrin coated pits. Boxed region is expanded in the lower left inset which shows the site (arrow) where an endocytic structure merges with the plasma membrane via a narrow opening. The upper right inset shows a similar structure as observed by traditional EM. (**I** and **J**) 3-dimensional model of the plasma membrane and endocytic intermediates derived from the tomographic series containing the section shown in panel H. (**J**) In this image, endocytic intermediates have been removed and white circles have been added to mark all sites where individual endocytic structures merge with the plasma membrane. The sites labeled as 1 and 2 are shown in more detail in panels H, K and L. (**K** and **L**) Reconstructed endocytic structures originating from sites 1 and 2 of panel J, superimposed on individual electron tomography sections to illustrate the site of connection with the rest of the plasma membrane. Scale bars: A-C, E, H-J= 250 nm, D, G, K and L=100 nm, H insets = 50 nm. See also Figure S6.

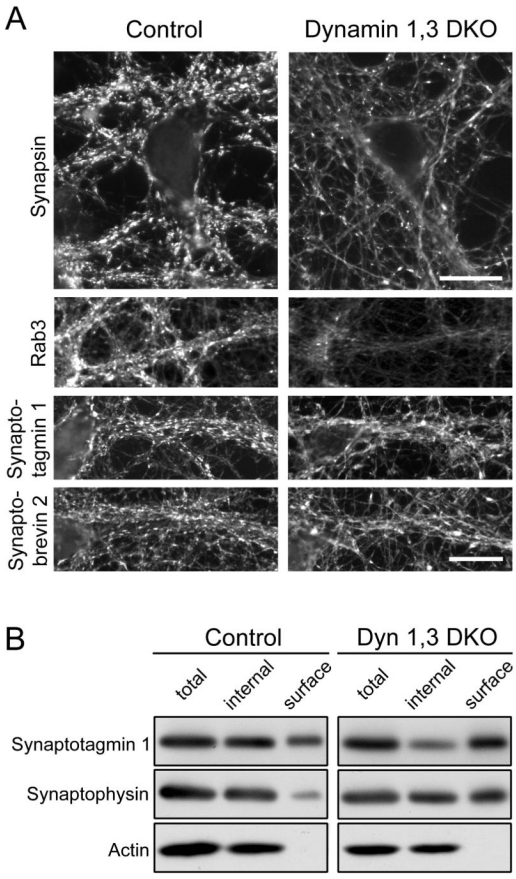

Figure 7.

Redistribution of synaptic vesicle proteins in DKO neurons. (**A**) Immunofluorescence for synapsin, Rab3, synaptotagmin 1 and synaptobrevin is highly punctate within presynaptic terminals in the control but is largely dispersed throughout the axons in the DKO sample. The additional loss of the Rab3 signal in the DKO parallels the decrease in the levels of this protein as detected by immunoblotting (Fig. 2E). (**B**) Cell surface biotinylation experiments show that the fractions of synaptotagmin 1 and synaptophysin which are surface exposed (biotinylated) are greatly increased in the DKO. As expected, actin is exclusively detected in the internal (non-biotinylated) fraction. Scale bars in (A) = 20μm.

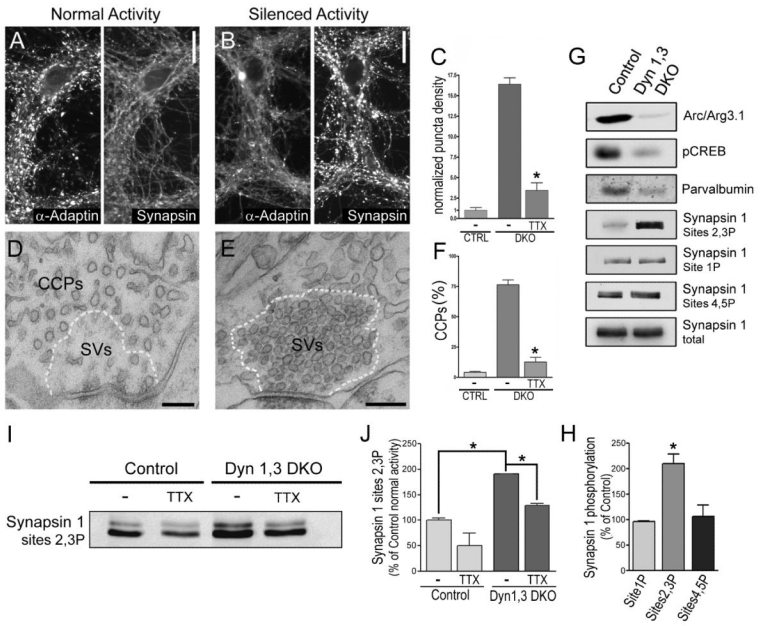

Figure 8.

Activity Dependence of the Endocytic Phenotype and Relationship to the Phosphorylation State of Synapsin 1 (**A**) a-Adaptin (left panel) and synapsin 1 (right panel) localization in DKO neurons under conditions of basal network activity. (**B**) a-Adaptin (left panel) and synapsin 1 (right panel) localization in DKO neurons after silencing of electrical activity with TTX (1 mM, 16 hr). (**C**) Quantification of presynaptic a-adaptin clustering in control neurons and DKO neurons under basal activity conditions and in DKO neurons after TTX treatment. (**D** and **E**) Electron micrographs of DKO synapses fixed under conditions of basal activity (D) and after TTX treatment (E). Dashed lines define a region adjacent to the active zone where synaptic vesicles are conspicuously absent in (D) but very abundant in (E). In contrast, clathrin-coated pits (CCPs) around this region are abundant in (D) but absent in (E). (**F**) Quantification of clathrin-coated pit (CCP) abundance in control neurons and DKO neurons under basal activity conditions and in DKO neurons after TTX treatment, expressed as the percentage of CCPs relative to the total of SVs + CCPs/synapse (n = 30 control, 35 DKO, and 37 TTX-treated DKO synapses). (**G**) Immunoblot analysis of activity-dependent changes in neuronal proteins of control and DKO cultures. (**H**) Quantification of the phosphorylation of synapsin 1 at the sites indicated (percentage of control) under basal activity levels in DKO cultures (n > 3). (**I** and **J**) Effect of neuronal network activity in controlling the levels of synapsin 1 phosphorylation at sites 2 and 3 and quantification of these results, respectively. $^{*}p < 0.01$, Student's t test. Scale bars represent 20 mm (A and B) and 200 nm (D and E). All data are presented as mean ± SEM.